Numerical Modelling of MT Fields in 2-D Anisotropic Structures with Topography and Bathymetry Considered

Josef Pek[1] and Hiroaki Toh[2]

[1]Geophysical Institute, Academy of Sciences of the Czech Republic
CZ-14131 Prague 4—Spořilov, Boční II/1401, Czech Republic

[2]Department of Earth Sciences, Faculty of Science, Toyama University
3190 Gofoku, Toyama 930-8555, Japan

Abstract

Motivated by the engagement of the second author of this study, Hiroaki Toh, in the Mantle Electromagnetic and Tomography (MELT) Experiment in the East Pacific, we modified our original 2-D magnetotelluric finite difference modelling procedure for generally anisotropic structures (Pek and Verner, 1997) to allow us to model MT data along topographic undulations as well as on the sea bottom. Both the topography and bathymetry are approximated by simple staircase functions. Introducing topography does not change the approximation procedure as compared to the flat earth model. The only difference is a variable bandwidth of the FD matrix in case of topography, which requires a slight modification to the Gaussian elimination procedure for the solution of the approximate problem. Modelling with bathymetry fits exactly into the standard modelling scheme, the specific being that MT fields and functions are evaluated inside the conductive medium rather than on the earth's surface. Large conductivity contrasts involved at sea-earth interfaces require to pay special attention to FD gridding. Improved derivative formulas according to Weaver *et al.* (1985, 1986) have been generalized to anisotropic models, which allows us to circumvent the inconsistency in boundary conditions for derived MT fields in heterogeneous media, as well as to increase the accuracy of the numerical evaluation of secondary fields and MT functions.

1 Introduction

Large-scale electrical macro-anisotropy has been recently recognized a real factor in several regional interpretations of MT data, the KTB being perhaps one of the examples most referred to in this respect (e.g., Eisel and Haak, 1999). The particular study presented here has been initiated by the second co-author of this contribution, Hiroaki Toh, who has taken part in collecting and interpreting MT data within the Mantle Electromagnetic and Tomography (MELT) Experiment (Evans *et al.*, 1999). The aim of the MT measurements within that project was to analyze the electrical resistivity structure of the mantle beneath the fast-spreading southern East Pacific Rise. Seismic data and some geoelectrical considerations indicate that the electrical anisotropy at mantle depths could be substantiated and might play a certain role in the electrical structure of the broader surrounding of the rift. As sea bottom MT measurements were employed in the experiment, a study on the influence of the anisotropy upon the deep sea MT data was encouraged. From a broader scope of aims of the related studies, we present here only the first results of a modified version of our 2-D MT modelling algorithm for anisotropic structures, which allows us to take into account both the topographic and bathymetric information available.

From the electrical point of view, the sea-land environment engenders some specific problems that are of particular relevance when modelling electromagnetic fields in this kind of setting, e.g.,

a) strong anomalous fields and currents can arise in the highly conductive sea water environment, which can produce severe distortions to the strongly attenuated primary fields, in particular on the sea bottom,

b) if anisotropic domains are involved, the intermode coupling due to anisotropy can be enhanced by the highly conductive sea water layer, and large distortions can appear, particularly if strike-perpendicular currents are transformed into strike-parallel currents,

b) large conductivity contrasts can cause serious numerical difficulties, especially when computing the secondary, derived electric and magnetic fields.

2 MT modelling for 2-D anisotropic structures with topography

In geophysical applications, finite element modelling codes are most often used to compute physical fields affected by general topographic features. High flexibility in choosing the particular shape of the finite elements, as well as easy accessibility to the gridding software for both the structured and unstructured meshes, make the finite elements much more suitable for dealing with complex geometries than the finite differences, where both serious theoretical and practical difficulties can arise when approximating fields in heterogeneous domains with complex geometrical boundaries.

Within the scope of finite difference techniques, topography is mostly included by approximating the topographic undulations by simple staircase functions that coincide piecewise with the FD grid lines. Though this approach may be problematic when modelling data directly on the slopes, it can yield useful results on platforms formed by several mesh steps along the topographic profile. There are more advanced techniques of including topographic features within the FD approximation, e.g., modifications to the FD stencil for oblique interfaces (e.g., Červ and Praus, 1972), or direct approximation procedures applied to general quadrilateral mesh cells, mostly based on mapping the approximate formulas for a rectangular cell onto a general tetragon (e.g., Hyman and Shishkov, 1999). In this paper, we still use the simplest staircase approximation to the surface undulations to estimate the topography effects.

2.1 Model and basic equations

A detailed description of the theory of the 2-D MT modelling for generally anisotropic structures has been given in (Pek and Verner, 1997). Here, we will only recapitulate the basic features of the mathematical model of the problem and the fundamental equations relevant to our further explanations.

In our model (Fig. 1), the conductive earth is approximated by a 2-D horizontally inhomogeneous halfspace, with the structural strike parallel to the x axis of the coordinate system. The z axis is directed down into the earth. A generally non-flat surface of the earth is assumed, with the topographic undulations conforming to the 2-D symmetry of the model. As modelling of sea-bottom experiments is considered, we explicitely assume that a part of the earth's surface is covered by a highly conductive sea water layer. The 2-D conductivity distribution within the earth can be generally anisotropic, specified by a symmetric and positive definite conductivity tensor $\sigma(y,z)$. We often factor the conductivity tensor by means of the diagonal matrix of the principal conductivities and three successive elementary Euler rotations (Verner and Pek, 1999), with a straightforward physical interpetation.

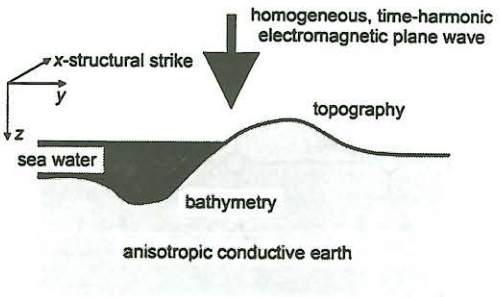

Figure 1: Sketch of the MT model.

The primary electromagnetic field is assumed to be a homogeneous, time-harmonic plane wave (time factor $\exp(-i\omega t)$) propagating from sources at $z \to -\infty$ towards the earth's surface. Slow enough electromagnetic processes are assumed for the quasi-steady state approximation of Maxwell's equations to be applicable.

For the MT model described above, the general Maxwell's equations can be reduced into two second-order partial differential equations for the basic, strike-parallel field components E_x and H_x,

$$\frac{\partial^2 E_x}{\partial y^2} + \frac{\partial^2 E_x}{\partial z^2} + i\omega\mu_0(\sigma_{xx} + \sigma_{xy}B + \sigma_{xz}A)E_x + i\omega\mu_0 A\frac{\partial H_x}{\partial y} - i\omega\mu_0 B\frac{\partial H_x}{\partial z} = 0, \tag{1}$$

$$\frac{\partial}{\partial y}\left(\frac{\sigma_{yy}}{D}\frac{\partial H_x}{\partial y}\right) + \frac{\partial}{\partial z}\left(\frac{\sigma_{zz}}{D}\frac{\partial H_x}{\partial z}\right) + \frac{\partial}{\partial y}\left(\frac{\sigma_{yz}}{D}\frac{\partial H_x}{\partial z}\right) + \frac{\partial}{\partial z}\left(\frac{\sigma_{yz}}{D}\frac{\partial H_x}{\partial z}\right) +$$
$$+ i\omega\mu_0 H_x - \frac{\partial}{\partial y}(AE_x) + \frac{\partial}{\partial z}(BE_x) = 0, \tag{2}$$

where

$$D = \sigma_{yy}\sigma_{zz} - \sigma_{yz}^2, \qquad A = (\sigma_{xy}\sigma_{yz} - \sigma_{xz}\sigma_{yy})/D, \qquad B = (\sigma_{xz}\sigma_{yz} - \sigma_{xy}\sigma_{zz})/D.$$

Though coupled, we conventially call eqs. (1) and (2) the E-mode equation and H-mode equation, respectively. The secondary, derived components of the electromagnetic field are obtained by simply

spatially differentiating the basic fields,

$$H_y = \frac{1}{i\omega\mu_0}\frac{\partial E_x}{\partial z}, \qquad H_z = -\frac{1}{i\omega\mu_0}\frac{\partial E_x}{\partial y},$$
$$E_y = \frac{\sigma_{yz}}{D}\frac{\partial H_x}{\partial y} + \frac{\sigma_{zz}}{D}\frac{\partial H_x}{\partial z} + BE_x, \qquad E_z = -\frac{\sigma_{yy}}{D}\frac{\partial H_x}{\partial y} - \frac{\sigma_{yz}}{D}\frac{\partial H_x}{\partial z} + AE_x. \tag{3}$$

Standard conditions on the contacts of domains with different conductivities, i.e., the continuity of the magnetic components, continuity of the tangential electric fields and of the normal current densities, as well as suitable conditions at infinite boundaries, complete the mathematical formulation of the model.

2.1.1 Finite volume FD approximation at topography nodes

The finite difference solution of the coupled system (1) and (2) by using the finite volume procedure consists in approximating the integral form of Maxwell's equations in a certain vicinity of the FD mesh nodes, rather than approximating directly the local, differential form of the field equations at respective nodes. By the finite volume approach, equations with spatially variable material parameters can be dealt with particularly easily as compared with the classical FD approaches.

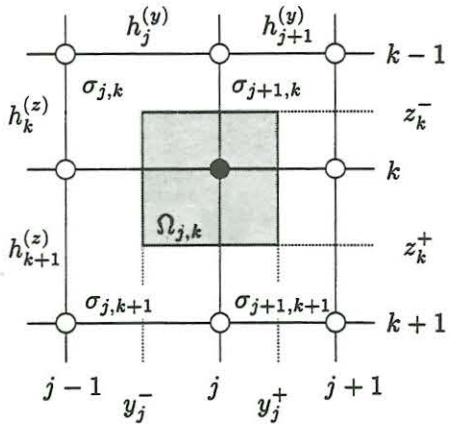

Figure 2: (j,k)-th mesh node and its vicinity. $\Omega_{j,k}$ is the (j,k)-th cell of a dual mesh with nodes defined by the centers of the basic FD mesh cells.

The finite volume approximation to (1), (2) was described in (Pek and Verner, 1997) in detail. The underlying physical model is covered by a non-uniform rectangular grid. The internal boundaries of domains with different conductivities are assumed to piecewise coincide with the grid lines of the FD mesh. Next, a dual mesh is constructed, with cells spanned over the centers of the primary FD mesh cells. The finite volume approximation to the basic equations (1), (2) is then carried out by integrating these equations over the cells of the dual mesh, surrounding the respective mesh nodes (see Fig. 2).

In (Pek and Verner, 1997), the corresponding FD stencils are given and their particular form is discussed for different positions of the mesh nodes with respect to the conductive medium and the non-conductive air for the case of a flat-earth model. Generally, equation (1) for E_x is approximated everywhere throughout the model, while eq. (2) is approximated at internal earth's nodes only, in virtue of the condition $H_x = \text{const}$ in the air that is assumed a perfect insulator. Introducing a general topography, approximated by a staircase function of the surface undulations conforming the underlying FD mesh, does not affect the finite volume approximation to (1), (2) at any position of the central mesh node. As the number of the internal mesh nodes within the conductor varies, however, in dependence on the topography, the number of H_x variables differs for different mesh columns. As a consequence, the band-width of the resulting FD matrix is variable—broader beneath topography elevations and narrower beneath topography depressions, as shown by a schematic example in Fig. 3. This is the only change to the algorithm that must be taken into account when dealing with structures with general topography. It affects slightly the Gaussian elimination procedure used for solving the FD equation system in that the maximum band-width of the FD matrix must be considered when storage is allocated for the elimination procedure.

3 Improved derivative formulas

In 2-D magnetotelluric models, both isotropic and anisotropic, the basic second order PDE's yield the primary, strike-parallel field components $E_x(y,z,\omega)$ and $H_x(y,z,\omega)$. The complete magnetotelluric field must be then constructed by evaluating the derived, secondary field components by differentiating the basic components with respect to the spatial coordinates y and z according to (3). The simplest way to do so is to interpolate the basic field components by a simple polynomial function and use the spatial derivatives of the interpolating polynom as approximations to the respective derivatives of the fields. This approach is widely used, e.g., with various kind of spline interpolators or, as in the original version of our anisotropic modelling code (Pek and Verner, 1997), with a three-point parabolic interpolation of the basic field values taken at three successive nodes of the numerical mesh in the y or z direction. In the latter case,

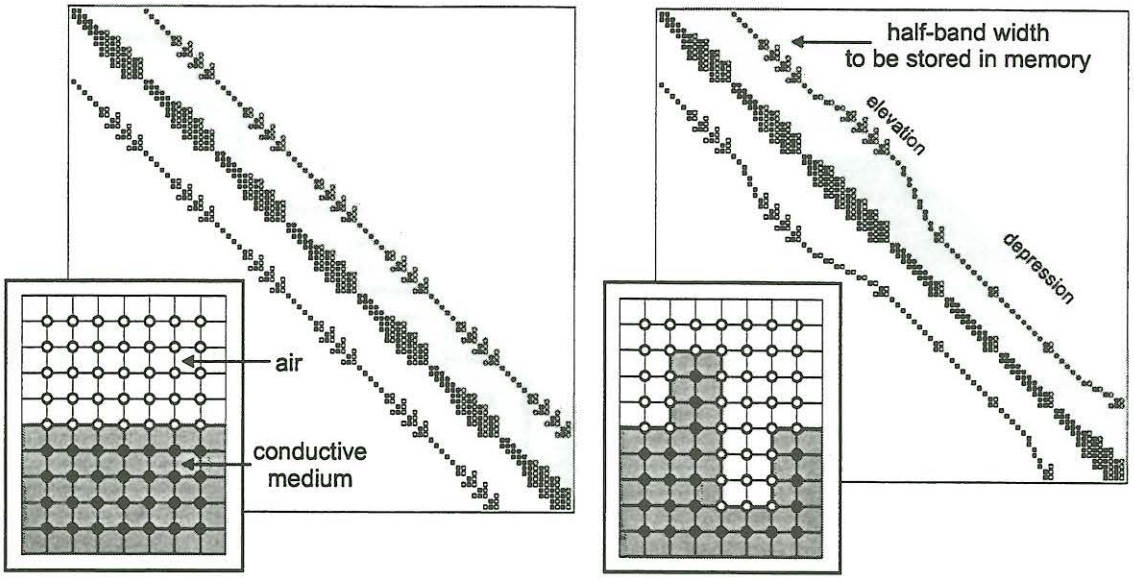

Figure 3: Structure of the FD matrix for the approximate solution of the 2-D MT problem with general anisotropy. Left panel: FD matrix for a flat earth model. Right panel: FD matrix for a model with general topography. The light gray zone shows the half-band width of the FD matrix that must be stored in the memory for solving the FD equations by the Gaussian elimination. Symbols used: full squares—coefficients for the electric field E_x, empty squares—coefficients for the magnetic field H_x. Symbols used in the insets: full circles—mesh nodes with only the electric field considered (air and surface nodes), empty circles—mesh nodes with both the electric and magnetic field considered (internal nodes within the conductive earth).

one-sided vertical derivatives of the magnetic field are used for the H-mode on the air-earth interface, obtained by fitting the interpolating parabola through the surface node and two nearest sub-surface nodes. Our experience with the simple parabolic interpolation shows that (i) for the E-polarization mode, the accuracy of the respective spatial derivatives decreases rapidly with increasing mesh steps, in particular at internal nodes surrounded by cells with large conductivity contrasts (see Fig. 4 for illustration), (ii) for the H-polarization mode, the accuracy of the derivatives is stable and sufficiently high for a broad range of mesh steps surrounding the 'derivative' node, mainly due to essentially a calmer spatial behaviour of the magnetic field. Nonetheless, using the one-sided parabolic interpolation in the H-mode case requires us to ensure that a sufficiently wide zone of uniform conductivity exists around the 'derivative' node so that the smoothness of the spatial derivatives conforms with the quadratic interpolation. Moreover, in the H-mode we have to face the inherent inconsistency of the classical solution to the field equations at joints where several blocks with different conductivities make contact: unless $\sigma_{j,k}\sigma_{j+1,k+1} = \sigma_{j+1,k}\sigma_{j,k+1}$ in a setting according to Fig. 2, we principally fail in meeting all the boundary conditions at interfaces surrounding the (j,k)-th node (i.e., the continuity of normal currents and continuity of tangential electric intensities). To circumvent this conflict requires a certain smoothing procedure to be applied locally to the conductivity distribution around the mesh node considered.

Weaver *et al.* (1985, 1986) recognized the above mentioned difficulties and gave a consistent solution to the problem of spatially differentiating the basic field components at a mesh node with the most general position possible within a rectangular mesh, i.e., at a mesh node surrounded by four mesh cells with generally different conductivities. Their approach to computing the spatial derivatives of the basic field components is based on the ideas of (i) re-shaping locally the electrical conductivity around the selected mesh node into a smooth conductivity distribution, without affecting the FD approximation of the underlying PDE, and, (ii) using the same approximation procedure to evaluate the derivatives as that they had used earlier in approximating the original PDE at the node considered.

The original procedure of Weaver *et al.* (1985, 1986) was based on the standard FD approximation approach which utilized the concept of fictitious, or virtual points to manage heterogeneous conductivity distributions around the mesh nodes. For anisotropic structures, however, that approach does not seem feasible. We will show here, however, that exactly the same derivative formulas can be obtained by using a much simpler finite volume approximation approach.

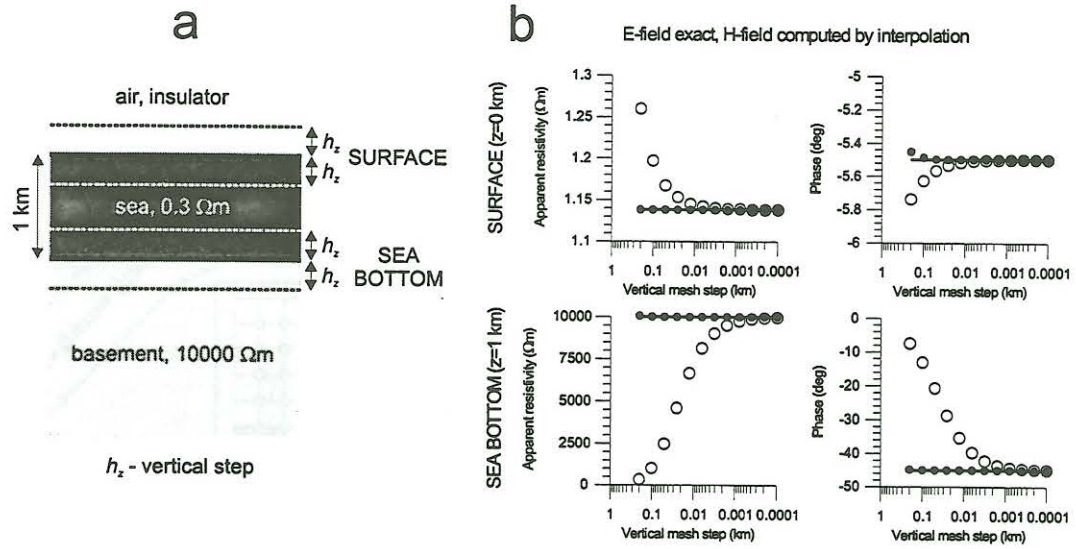

Figure 4: Comparison of 1-D apparent resistivities and phases computed from exact electric components and approximate magnetic components. (a) 1-D model with a sea layer (1 km thick, 0.3 Ωm) and a resistive basement (10000 Ωm). (b) Apparent resistivities (left panels) and phases (right panels) on the surface (top panels) and on the sea bottom (bottom panels) for different mesh steps around the central node. The exact MT functions (full line) are compared with corresponding functions computed from approximate magnetic fields obtained by a parabolic interpolation of the electric components through three nodes (empty circles) and by using improved derivative formulas by Weaver *et al.* (1986) (full circles).

3.1 Improved derivative formulas for anisotropic 2-D models

3.1.1 Spatial derivatives of E_x at internal mesh nodes

After FD approximating the second order coupled equations (1) and (2), we can solve the FD linear system for the approximation to E_x and H_x throughout the model. To compute the derived magnetic fields, H_y and H_z, according to corresponding formulas in (3), the basic idea of Weaver *et al.* (1986) was (i) to use Taylor's expansion, into the second order in the respective mesh step, of the basic field E_x in two oposite directions from the central node, (ii) substitute the second derivatives in those expansions for their equivalents from the original second order equation, and, after (iii) properly averaging the conductivities at either side of the central node, (iv) eliminate the remaining second derivative of E_x by subtracting the suitably scaled equations from the previous steps. In the anisotropic case, the influence of the magnetic field H_x must be considered as well, which may affect essentially the conductivity averaging procedure. Most of the discussion on averaging the conductivities or resistivities over the integration cell $\Omega_{j,k}$ can be repeated, with only slight modifications, for the anisotropic case as well. The most significant change is that the individiual components of the current densities are not given by simply multiplying the corresponding electric fields by the scalar conductivity, but depend generally on all the electric components via a conductivity tensor multiplication. The boundary conditions at the interfaces that divide domains with different conductivity tensors must be modified appropriately.

As the fictitious points FD approximation procedure is difficult to use in the anisotropic case, we will demonstrate that Weaver's *et al.* (1986) derivative formulas, and their generalized versions for anisotropic conductivities, can be easily obtained by applying the principles of the finite volume approximation, which we used earlier to approximate the anisotropic 2-D problem in (Pek and Verner, 1987). For evaluating, e.g., the vertical derivative, $\partial E_x(y_j, z_k)/\partial z$, the idea is to apply the volume integration of (1) separately to the upper (i.e. $z > z_k$) and lower (i.e. $z < z_k$) sub-cell of the original integration cell $\Omega_{j,k}$ (Fig. 2), and to subtract the resulting integrals in order to eliminate the horizontal field derivatives involved. Let us integrate

$$I_E(\Omega_{j,k}, z_k-) =$$

$$= \int_{y_j^-}^{y_j^+} \int_{z_k^-}^{z_k} \left[\frac{\partial^2 E_x}{\partial y^2} + \frac{\partial^2 E_x}{\partial z^2} + i\omega\mu_0(\sigma_{xx} + \sigma_{xy}B + \sigma_{xz}A)E_x + i\omega\mu_0 A \frac{\partial H_x}{\partial y} - i\omega\mu_0 B \frac{\partial H_x}{\partial z} \right] dy\, dz \approx$$

$$\approx \frac{h_k^{(z)}}{2}\,\frac{E_x(j+1,k)-E_x(j,k)}{h_{j+1}^{(y)}} - \frac{h_k^{(z)}}{2}\,\frac{E_x(j,k)-E_x(j-1,k)}{h_j^{(y)}} + \frac{h_j^{(y)}+h_{j+1}^{(y)}}{2}\,\frac{\partial E_x(j,k)}{\partial z} +$$

$$- \frac{h_j^{(y)}+h_{j+1}^{(y)}}{2}\,\frac{E_x(j,k)-E_x(j,k-1)}{h_k^{(z)}} + \frac{i\omega\mu_0}{4} h_k^{(z)}(h_j^{(y)}+h_{j+1}^{(y)})\sigma^-(j,k)E_x(j,k) +$$

$$+ \frac{i\omega\mu_0}{4} h_k^{(z)}\left\{A_{j+1,k}\left[H_x(j+1,k)-H_x(j,k)\right] + A_{j,k}\left[H_x(j,k)-H_x(j-1,k)\right]\right\} -$$

$$- \frac{i\omega\mu_0}{4}(h_j^{(y)}B_{j,k} + h_{j+1}^{(y)}B_{j+1,k})\left[H_x(j,k)-H_x(j,k-1)\right] = 0,$$

where

$$\sigma^-(j,k) = \frac{h_j^{(y)}\Sigma_{j,k} + h_{j+1}^{(y)}\Sigma_{j+1,k}}{h_j^{(y)}+h_{j+1}^{(y)}}, \qquad \Sigma = \sigma_{xx} + \sigma_{xy}B + \sigma_{xz}A,$$

and a short notation, e.g., $E_x(y_j, z_k) \equiv E_x(j,k)$, has been used. The steps used in approximating the above integral are identical with those applied earlier to the finite volume approximation of (1) in (Pek and Verner, 1997). Similarly, we can also approximate the complementary integral $I_E(\Omega_{j,k}, z_k+)$ over the upper half-cell of $\Omega_{j,k}$, i.e., over the domain $\langle y_j^-, y_j^+\rangle \times \langle z_k, z_k^+\rangle$.

To eliminate the approximate expressions for the horizontal derivatives and extract the vertical derivative $\partial E_x(j,k)/\partial z$, we evaluate the expression $2h_{k+1}^{(z)} I_E(\Omega_{j,k}, z_k-) - 2h_k^{(z)} I_E(\Omega_{j,k}, z_k+)$, and finally obtain, after some algebra, the following approximation

$$\frac{\partial E_x(j,k)}{\partial z} \approx \frac{1}{h_k^{(z)}+h_{k+1}^{(z)}}\left\{\frac{h_k^{(z)}}{h_{k+1}^{(z)}}\left[E_x(j,k+1)-E_x(j,k)\right] + \frac{h_{k+1}^{(z)}}{h_k^{(z)}}\left[E_x(j,k)-E_x(j,k-1)\right]\right\} +$$

$$+ \frac{i\omega\mu_0}{2}\,\frac{h_k^{(z)}h_{k+1}^{(z)}}{h_k^{(z)}+h_{k+1}^{(z)}}\left[\sigma^+(j,k)-\sigma^-(j,k)\right]E_x(j,k) +$$

$$+ \frac{i\omega\mu_0}{2}\,\frac{h_k^{(z)}h_{k+1}^{(z)}}{(h_j^{(y)}+h_{j+1}^{(y)})(h_k^{(z)}+h_{k+1}^{(z)})}\left\{(A_{j+1,k+1}-A_{j+1,k})[H_x(j+1,k)-H_x(j,k)] + \right. \qquad (4)$$

$$\left. + (A_{j,k+1}-A_{j,k})[H_x(j,k)-H_x(j-1,k)]\right\} -$$

$$- \frac{i\omega\mu_0}{2}\,\frac{1}{h_k^{(z)}+h_{k+1}^{(z)}}\left\{h_k^{(z)}B^+(j,k)[H_x(j,k+1)-H_x(j,k)] - h_{k+1}^{(z)}B^-(j,k)[H_x(j,k)-H_x(j,k-1)]\right\},$$

with

$$B^-(j,k) = \frac{h_j^{(y)}B_{j,k} + h_{j+1}^{(y)}B_{j+1,k}}{h_j^{(y)}+h_{j+1}^{(y)}}, \qquad B^+(j,k) = \frac{h_j^{(y)}B_{j,k+1} + h_{j+1}^{(y)}B_{j+1,k+1}}{h_j^{(y)}+h_{j+1}^{(y)}}.$$

The first two terms of (4) contain the E_x field only, and are identical with the corresponding Weaver's *et al.* (1986) improved derivative formula derived for the isotropic case (except for the reversed sign of $i\omega\mu_0$, resulting from our using the $\exp(-i\omega\mu_0)$ time-harmonic factor). The first term in (4) represents a derivative as it would result from a simple parabolic interpolation of E_x through the mesh nodes $(j,k-1)$, (j,k), and $(j,k+1)$. The second term is a correction that results from considering the original PDE in expressing the second-order derivative $\partial^2 E_x/\partial z^2$. This correction is directly proportional to the difference of avarage conductivities below and above the central mesh node, and, for large conductivity contrasts, neglecting this correction term can result in a fatal drop of the accuracy of the derived fields, even if the basic field component E_x is available exactly, or with a very high precision. Fig. 4 illustrates that for a sea layer 1 km thick, a sea/basement resistivity contrast of 0.3/10000, and the period of 100 s, the vertical mesh step would have to be *less then 1 meter* at the sea bottom to provide sufficiently accurate MT functions by using the parabolic interpolation formula alone. Considering standard gridding rules used in the MT modelling, this would result in enormous mesh dimensions, hardly tractable in practice even for the simplest models.

The remaining two terms in (4) involve the magnetic component H_x, and express the influence of the H-mode field upon E_x via the inter-mode coupling in the anisotropic case. These terms depend on the non-diagonal elements of the conductivity tensor via the aggregate parameters A and B and their averages B^- and B^+.

To get an analogous formula for the horizontal derivative $\partial E_x(j,k)/\partial y$, it would be now easy to repeat the above procedure, with computing and subtracting the integrals $I_E(\Omega_{j,k}, y_j-)$ and $I_E(\Omega_{j,k}, y_j+)$ over the left-hand and right-hand sub-cells of the integration cell $\Omega_{j,k}$.

3.1.2 Spatial derivatives of H_x at internal mesh nodes, derived electric fields E_y, E_z

The procedure for evaluating the derived electrical components E_y and E_z from (3) is similar to that used in the previous section, only the finite volume integration is now applied to the basic equation (2). Contrary to the previous case, we must, however, realize that the conductivity averaging involved in the quasi-H-mode case is of a more principal nature: As for the setting in Fig. 2 it is not generally possible to find a consistent set of electric fields E_y and E_z and current densities j_y and j_z within the cell $\Omega_{j,k}$, we have to re-shape the local conductivity distribution around the node (j,k) in such a way that we eliminate those sharp boundaries within $\Omega_{j,k}$ that would lead to inconsistencies in the local boundary conditions.

Without going into detail, the finite volume integration of (2) over the lower and upper half-cell of $\Omega_{j,k}$, and subsequent subtraction of the properly scaled integrals allows us to extract a mean tangential component of the electric field over the interval $\langle y_j^-, y_j^+ \rangle \times z_k$, i.e., $\bar{E}_y(j,k)$, and express it in a general symbolic form

$$\bar{E}_y(j,k) = \frac{2}{h_j^{(y)} + h_{j+1}^{(y)}} \int_{y_j^-}^{y_j^+} E_y(y, z_k)\, dy \approx$$

$$\approx \frac{\varrho_{yy}^-(j,k)\varrho_{yy}^+(j,k)}{(h_k^{(z)} + h_{k+1}^{(z)})\varrho_{yy}(j,k)} \sum_{\iota=j-1}^{j+1} \sum_{\kappa=k-1}^{k+1} \left[C_{\iota,\kappa}^H H_x(\iota,\kappa) + C_{\iota,\kappa}^E E_x(\iota,\kappa) \right], \tag{5}$$

where $\varrho_{yy}^-(j,k)$, $\varrho_{yy}^+(j,k)$, and $\varrho_{yy}(j,k)$ are averaged yy-resistivities over the upper and lower half-cell and over the whole cell $\Omega_{j,k}$, respectively. The coefficients $C_{\iota,\kappa}^H$ and $C_{\iota,\kappa}^E$ in (5) are complex functions of the conductivities and mesh steps, and we are not going to give their explicit form here.

It can be shown that the mean tangential component $\bar{E}_y(j,k)$ in (5) is generally given by both the electric and magnetic fields that enter the 9-point-H/5-point-E FD stencil resulting from the approximation of (2) by the finite volume method (Pek and Verner, 1997). It can be proved that for an isotropic cell, the above formula reduces into Weaver's *et al.* (1985) expression for $\bar{E}_y(j,k)$.

Similarly as above, we can also obtain an approximate formula for the mean vertical field $\bar{E}_z(j,k)$.

3.2 Derivative formulas at topography nodes

So far, the formulas for the spatial derivatives have been considered under the assumption that the nodal point (j,k) was an *internal* point of the medium, i.e., that it was fully surrounded by cells with non-zero conductivity tensor elements. If some of the mesh cells that surround the mesh node (j,k) contain a perfect insulator, i.e., mostly air in our applications, the derivative formulas must be modified accordingly. Formally, we can get the modified formulas by taking the general expressions (4) or (5) and evaluating their limits for the conductivity, or resistivity, of the air cells approaching zero, or infinity, respectively. This approach leads to consistent formulas, except for few situations that cannot be dealt with in this way. In particular, evaluating $\bar{E}_z$ on a flat earth surface, or $\bar{E}_y$ on a vertical wall leads to an indefinite limit 0/0. Those special situations are, however, of only limited interest for the MT practice.

4 Examples of numerical simulations

In this section, we will briefly discuss two simple numerical examples that were used as tests for the developed algorithm for the 2-D MT modelling for anisotropic models with topography and bathymetry considered. Both models represent variants of a simple horst model; in the first example a horst as a topographic elevation, in the second example a horst as an undersea elevation or an island.

4.1 Topography: effect of a horst on MT fields

First, we consider a two-layer model with the following parameters: $h_1 = 125$ km, $\varrho_1 = 1000$ Ωm; $\varrho_2 = 200$ Ωm. On the top of the upper layer, a block elevation is located with the width of 44 km and height of 1 km. The resistivity within the elevated block is equal to that of the undelying layer, i.e., 1000 Ωm. In Fig. 5, top (panel ISO), a snapshot of the electric field E_x for the E-mode and the magnetic field H_x for the H-mode is displayed for the period of 100 s. The plots show that there is only a weak influence of the elevation upon the magnetic component H_x, expressed by an almost uniform offset of the contours towards the elevated surface, with diminishing tendency towards greater depths. A very weak local concentartion of the E_x field occurs immediately above the horst.

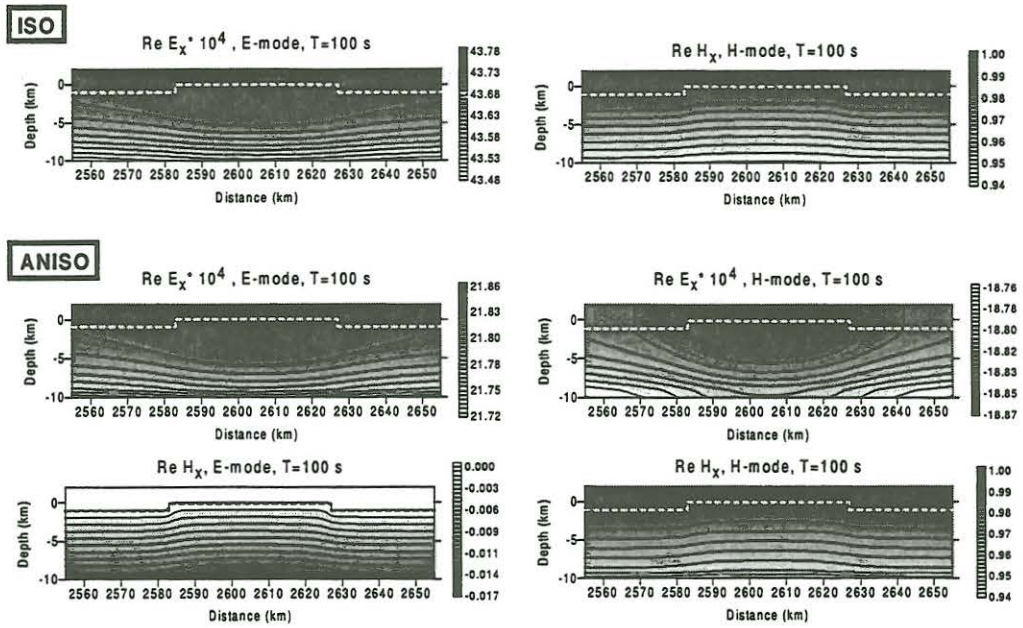

Figure 5: Effect of a resistive horst, 44 km wide and 1 km high, upon the magnetotelluric fields E_x and H_x for the period of 100 s. Top panels (ISO): Snapshots of MT fields for an isotropic basement. Bottom panels (ANISO): MT fields for a model with a highly anisotropic crust and upper mantle. For the model specifications, see the text.

As to the topography effect on the MT curves, both the apparent resistivities and phases show only a very weak effect of the elevation. Within the period range of 0.3 to 3000 s, the MT anisotropy does not exceed the value of 1.1, except points in the immediate vicinity of the edges of the horst, where the H-mode resistivities display a pronounced static shift effect due to the jump in topography. Above the elevation, a slight increase of the E-mode resistivity occurs, corresponding to the local thickening of the resistive layer.

Next experiment involved a highly anisotropic upper crustal layer that interrupted the 1000 Ωm resistive layer from the previous model within the depth interval of 2 to 9 km. The principal resistivities of the anisotropic layer were 10/1000/10 Ωm and the anisotropy strike was 60 deg with respect to the structural strike. The bottom panel (ANISO) in Fig. 5 shows the snapshot of the E_x and H_x field distribution for the quasi-E and quasi-H field modes, i.e., for the primary magnetic field directed parallel to the y and x axis, respectively. For the quasi-E-mode (left panels of ANISO), the E_x field is very similar to that obtained in the isotropic case, except for its size that is about a half of the respective isotropic field. A part of the energy is transformed into the perpendicular mode by the effect of anisotropy. The quasi-H-mode field distribution (right panels of ANISO) gives an idea about the size of the electric field arising due to the anisotropy coupling—in this case, E_x is comparable, as to the order of magnitude, with the electric field of primary origin in the quasi-E-mode.

Similarly as in the isotropic case, the effect of the topographic elevation above a highly anisotropic basement on the MT curves is again very weak, and is most expressed by static shifts of apparent resistivities in the immediate vicinity of the edges of the horst. Similar behaviour has been observed for models with a rougher topography as well, though their practical significance is rather limited owing to a largely simplified staircase approximation of the topographic undulations.

4.2 Bathymetry: effect of an undersea horst on sea-bottom MT measurements

For numerical simulations of an MT experiment with bathymetry considered, we have used a similar model as in the above topography study, with the horst surrounded now by a higly conductive layer, simulating the sea water. An anisotropic layer has been placed into upper mantle depths. The structure of the model used is shown in Fig. 6. Various heights of the horst were chosen, from zero (flat sea bottom) up to 1 km (model ISLAND). MT functions have been evaluated along the surface of the model as well as along the bathymetry profile, i.e., along the sea bottom at those sections of the model covered by the sea water, and along the surface elsewhere.

As an example of modelling results, we present the MT profile curves across the ISLAND model for the period of 100 s in Fig. 7. For this period, the manifestation of the deep anisotropic layer is negligible, but we can observe some interesting phenomena related to the undersea topography.

The surface MT data (bottom panels in Fig. 7) show a standard course as observed along a shallow highly conductive layer interrupted by a resistive intrusion. The sea bottom MT curves show a more intricate behaviour, especially in the E-mode. The E-mode resistivity (xy-curve) steeply increases away from the edge of the elevation, reaching a maximum at about 50 km from the verge of the horst. From this maximum, the resistivity decreases back to the corresponding 1-D boundary value for large distances from the horst. Near the resistivity maximum, the phase curves show a highly anomalous behaviour, and even leave locally their 'natural' quadrant. To eliminate the possibility of numerical effects in this case, where large conductivity contrasts might lead to inaccuracies in evaluating especially the derived fields, we compared our modelling results with those obtained by independent calculations carried out by Yuguo Li's FE algorithm (Li, 2000). The comparison tests have given practically identical results. Both sets of model curves are presented in Fig. 7.

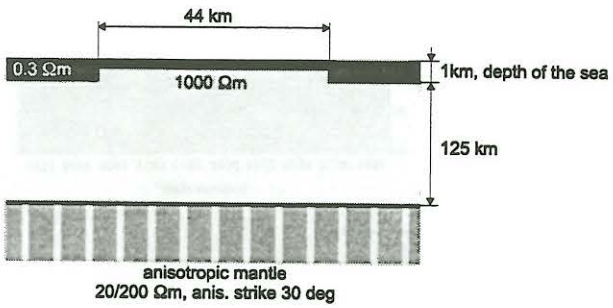

Figure 6: Model used for the sea bottom MT modelling studies.

The above anomalous effect of the E-mode MT curves is observed for a broad range of elevation heights, and is not restricted to the ISLAND model only. The model tests with the field distributions across the sea layer indicate that anomalous current concentrations appear in the highly conductive sea along the edges of the elevation. The magnetic fields of these anomalous currents can locally reduce, or even revert, the total magnetic field on the sea bottom, which, in turn, results in an anomalous increase of the impedance and its anomalous phase shift along a certain portion of the sea bottom profile away from the elevation.

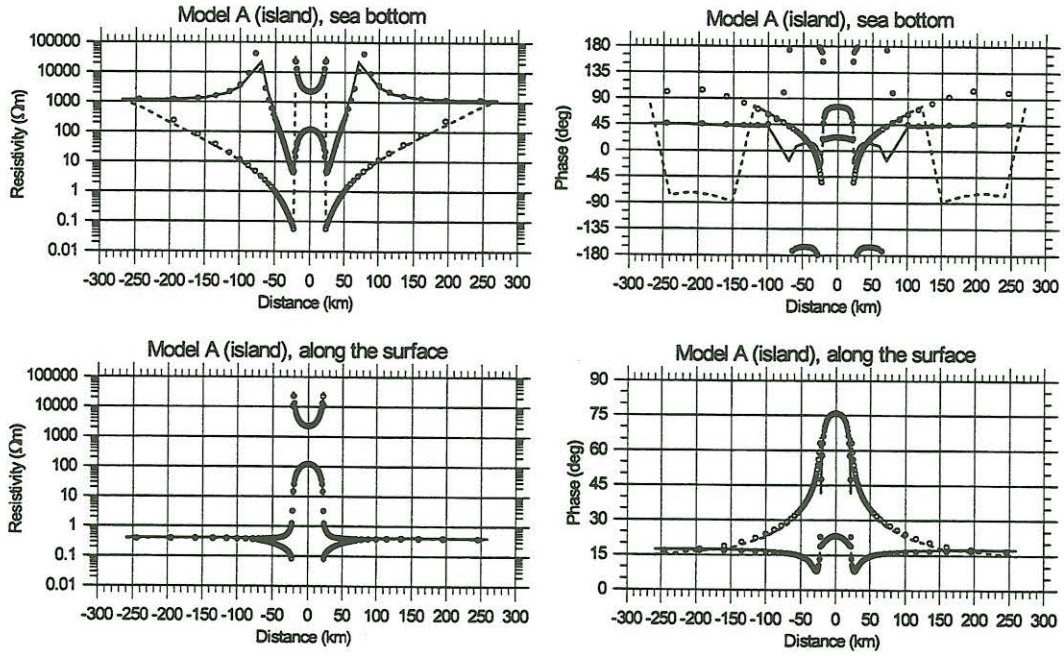

Figure 7: Apparent resistivities and phases for the model from Fig. 6, with the undersea elevation reaching up to the sea level (model ISLAND), for the period of 100 s. Top panels: MT functions along the sea bottom (except the island section, where the surface values are given). Bottom panels: MT functions along the surface. Symbols used: full circles—xy curves, empty circles—yx curves, full lines—xy curves computed by the FE algorithm of Yuguo Li (2000), dashed lines—yx curves computed by the same algorithm. The discrepancies between the phase curves produced by the two algorithms used along the sea bottom represent only 90 deg shifts, and result from different coding conventions for the evaluation of the MT phases in the codes compared.

5 Conclusion

We have presented here a simple generalization of our 2-D MT modelling algorithm for anisotropic structures (Pek and Verner, 1997) to models with topography and bathymetry. If both the topographic and bathymetric undulations are approximated by simple staircase functions, conforming with the underlying FD mesh, no substantial modifications to the FD approximation procedure are required as compared with the flat-earth model. The only change concerns the variable band-width of the FD matrix in case of a variable topography in our algorithm, which requires us to slightly modify the Gaussian elimination procedure used for the solution of the FD equation system.

A more serious point seems to be the question of evaluating the derived field components from the basic, strike-parallel fields E_x and H_x. Here, large numerical errors may be expected to occur at large conductivity contrasts, especially if traditional simple interpolation formulas are used to compute the spatial derivatives of the basic fields. The generalization of Weaver's *et al.* (1985, 1986) improved derivative formulas to anisotropic models seems to be a crucial point in extending the anisotropy modelling to the sea bottom MT simulations.

Although only simple schematic simulation models have been chosen to illustrate the numerical technique developed, there is a lesson not to underestimate, particularly for the deep sea MT modelling. The simple undersea elevation model, presented in the last section, predicts a highly anomalous behaviour of the sea bottom MT data relatively far away from the edges of the horst. Although checked by two independent modelling procedures, that phenomenon has not yet been verified on practical data. Nevertheless, the example shows that the high mobility of electric currents in the highly conductive sea environment, along with a strong attenuation of the primary field, can produce serious distortions to the deep sea MT fields. More extensive modelling and, in particular, a confrontation of the models with real MT data are, however, required to understand those phenomena more comprehensively.

Acknowledgement

This research has been supported by the Grant Agency of the Czech Republic under the contract No. 205/99/0917. Our thanks goes to Yuguo Li who kindly carried out computations necessary for the comparison tests of our modelling code.

References

Červ, V. and O. Praus, 1972, MT-field of H-polarization in models with dipping interfaces, *Studia geoph. et geod.*, **16**, 285.

Eisel, M. and V. Haak, 1999, Macro-anisotropy of the electrical conductivity of the crust: a magnetotelluric study of the German Continental Deep Drilling site (KTB), *Geophys. J. Int.*, **136**, 109–122.

Evans, R. L., P. Tarits, A. D. Chave, A. White, G. Heinson, J. H. Filloux, H. Toh, N. Seama, H. Utada, J. R. Booker and M. J. Unsworth, 1999, Assymetric electrical structure in the mantle beneath the East Pacific Rise at 17°S, *Science*, **286**, 752–756.

Hyman, J. M. and M. Shashkov, 1999, Mimetic discretizations for Maxwell's equations, *J. Comp. Phys.*, **151**, 881–909.

Li, Y., 2000, Finite element modelling of magnetotelluric fields in 2-D structures with arbitrary anisotropy, in this volume.

Pek, J. and T. Verner, 1997, Finite-difference modelling of magnetotelluric fields in two-dimensional anisotropic media, *Geophys. J. Int.*, **128**, 505–521.

Verner, T. and J. Pek, 1998, Numerical modelling of direct currents in 2-D anisotropic structures, in: Bahr, K. and Junge, A. (eds.): *Protokoll über das Kolloquium "Elektromagnetische Tiefenforschung", Neustadt/Weinstraße, Germany, 9.-13.3.1998*, DGG, 228–237.

Weaver, J. T., V. B. Le Quang and G. Fischer, 1985, A comparison of analytical and numerical results for a two-dimensional control model in electromagnetic induction—I. B-polarization calculations, *Geophys. J. R. astr. Soc.*, **82**, 263–278.

Weaver, J. T., V. B. Le Quang and G. Fischer, 1986, A comparison of analytical and numerical results for a 2-D control model in electromagnetic induction—I. E-polarization calculations, *Geophys. J. R. astr. Soc.*, **87**, 917–948.